Quantifying the dynamics of HIV decline in perinatally-infected neonates on antiretroviral therapy

Sinead E. Morris[*1] (PhD), Luise Dziobek-Garrett[1†] (MSc), Renate Strehlau[2] (MBBCh), Juliane Schröter[3] (MSc), Stephanie Shiau[4,5] (PhD, MPH), Anet J. N. Anelone[3‡] (PhD), Maria Paximadis[6] (PhD), Rob J. de Boer[3] (PhD), Elaine J. Abrams[5,7,8] (MD), Caroline T. Tiemessen[6] (PhD), Louise Kuhn[4,5] (PhD, MPH), Andrew J. Yates[*1] (PhD), on behalf of the EPIICAL Consortium and the LEOPARD study team.

[1]Department of Pathology and Cell Biology, Columbia University Medical Center, New York, NY, USA
[2]Empilweni Services and Research Unit, Rahima Moosa Mother and Child Hospital, Department of Paediatrics and Child Health, Faculty of Health Sciences, University of the Witwatersrand, Johannesburg, South Africa
[3]Department of Theoretical Biology and Bioinformatics, Utrecht University, Utrecht, Netherlands
[4]Gertrude H. Sergievsky Center, Vagelos College of Physicians and Surgeons, Columbia University Medical Center, New York, NY, USA
[5]Department of Epidemiology, Mailman School of Public Health, Columbia University Medical Center, New York, NY, USA
[6]Centre for HIV and STIs, National Institute for Communicable Diseases, National Health Laboratory Services, and Faculty of Health Sciences, University of the Witwatersrand, Johannesburg, South Africa
[7]ICAP at Columbia University, Mailman School of Public Health, Columbia University Medical Center, New York, NY, USA
[8]Department of Pediatrics, Vagelos College of Physicians & Surgeons, Columbia University Medical Center, New York, NY, USA

* **Corresponding authors:** Sinead E. Morris and Andrew J. Yates
Department of Pathology and Cell Biology, Columbia University Medical Center, New York, NY, USA
Email: `sinead.morris@columbia.edu` and `andrew.yates@columbia.edu`

†**Present address:** Office of University Investments, Cornell University, New York, NY, USA
‡**Present address:** School of Mathematics and Statistics, University of Sydney, Sydney, Australia

Supplementary Information

Data

All baseline covariates in the original dataset are as follows: infant follow up status, age at last study visit, sex, delivery mode, weight at birth, prevention of mother-to-child transmission (PMTCT) interventions, whether the birth was preterm, initial CD4 percentage, initial CD4 count, age of mother, mother's viral load (VL) at

birth, mother's CD4 count at birth, the initial ART regimen, the age at which ART was initiated, and the age at which the regimen was changed.

Of the 53 infants included in our analysis, 49 were initially prescribed a drug regimen of three reverse transcriptase inhibitors (RTIs): nevirapine, lamivudine, and zidovudine. The exceptions were four infants initially treated with a protease inhibitor (PI), ritonavir boosted lopinavir, and two RTIs: two infants received lamivudine and abacavir, and two received lamivudine and zidovudine. After a median age of 31 days, all infants were switched to a PI-based regimen.

Model

The following ODE system describes the dynamics of HIV infection and treatment. Uninfected target cells, T, are infected by free virions at per-capita rate k to become short-lived infected cells, T^*. These cells produce virions at rate p and die at rate δ. Other cells, M, can also become infected at per-capita rate k_M, resulting in long-lived infected cells, M^*. These long-lived infected cells also produce virions at rate p and die at rate $\gamma < \delta$. Virions can either be infectious (i.e. capable of infecting new cells), V_I, or non-infectious, V_{NI}, and decay at rate $c \gg \delta, \gamma$. Assuming a reverse-transcriptase inhibitor blocks infection of new cells with efficacy e_1 and a protease inhibitor blocks the production of infectious virions with efficacy e_2, we can write the following equations

$$\frac{dT^*}{dt} = (1-e_1)kTV - \delta T^* \tag{S1}$$
$$\frac{dM^*}{dt} = (1-e_1)k_M MV - \gamma M^* \tag{S2}$$
$$\frac{dV_I}{dt} = (1-e_2)(pT^* + pM^*) - cV_I \tag{S3}$$
$$\frac{dV_{NI}}{dt} = e_2(pT^* + pM^*) - cV_{NI}, \tag{S4}$$

as outlined previously [1–4]. Note that for any $e_2 \in [0,1]$, the total number of free virions, V, is given by

$$\begin{aligned}\frac{dV}{dt} &= \frac{dV_I}{dt} + \frac{dV_{NI}}{dt} \\ &= (1-e_2)(pT^* + pM^*) + e_2(pT^* + pM^*) - c(V_I + V_{NI}) \\ &= pT^* + pM^* - cV.\end{aligned}$$

Thus, the efficacy of the protease inhibitor has no observable impact on the combined dynamics of infectious and non-infectious virions.

Now, assuming that viral dynamics occur on a faster timescale than infected cells, we can make the quasi-steady state assumption that $dV/dt \approx 0$, so that

$$V(t) = \tfrac{p}{c}\big(T^* + M^*\big). \tag{S5}$$

Finally, if we assume reverse transcriptase inhibition is completely effective (i.e. $e_1 = 1$), we can solve Eqns S1 and S2 to give $T^* = T_0 e^{-\delta t}$ and $M^* = M_0 e^{-\gamma t}$, were T_0 and M_0 are the initial numbers of short and long-lived infected cells (i.e. $T(t = 0)$ and $M(t = 0)$), respectively. Substituting these solutions into Eqn. S5 gives the final expression

$$V(t) = Ae^{-\delta t} + Be^{-\gamma t},$$

where $A = pT_0/c$ and $B = pM_0/c$. In other words, viral load should decay exponentially with an initial phase of rapid decline, reflecting the loss of short-lived infected cells (δ), and then enter a second, slower decline phase, reflecting the loss of long-lived infected cells (γ). Finally, note that $A/(A + B) = T_0/(T_0 + M_0)$ i.e. the proportion of the total initial infected cell population that is short-lived.

To estimate when the transition from the first to the second phase occurs, we can identify the time, T_t, at which the rates of change of the two phase terms are equivalent [5]. More formally, we solve the equation

$$\frac{d}{dt}(Ae^{-\delta t}) = \frac{d}{dt}(Be^{-\gamma t}),$$

which leads to the expression

$$A\delta e^{-\delta T_t} = B\gamma e^{-\gamma T_t}.$$

Taking the log of both sides,

$$\log(A\delta) - \delta T_t = \log(B\gamma) - \gamma T_t,$$

and then rearranging

$$\log(A\delta) - \log(B\gamma) = \delta T_t - \gamma T_t,$$

gives

$$T_t = \frac{\log(A\delta) - \log(B\gamma)}{\delta - \gamma}.$$

Alternative censoring values

In the main text we set all measurements below the 20 copies ml^{-1} detection threshold of the RNA assay to 10 copies ml^{-1}, in line with previous work [6]. Using other levels of censoring had minimal impact on our results. For example, the median short-lived lifespan estimate from the biphasic model was largely unchanged when setting censored values to 1, 5, or 15 copies ml^{-1}, rather than 10 copies ml^{-1} (Fig. S6). Although median estimates of the long-lived lifespan and time to suppression increased with increasing censored value, this effect was small, and is expected given that reducing the censored value will create a sharper decay slope at the very

final stages of suppression.

Sustained suppression criteria

In the main text we define viral suppression to be the presence of at least one VL measurement below the detection threshold (referred to here as the 'original' criterion). We also investigated the stricter definition that infants must have two consecutive measurements below the threshold (referred to as the 'sustained' criterion). Of the 43 infants fit using the original criterion, 33 met the stricter sustained criterion: 6 were fit using the biphasic model (Fig. S7) and 27 using the single phase model (Fig. S8). Of the 53 infants that met the original criterion for calculating the non-parametric time to suppression (TTS), 39 of these also met the sustained criterion.

For the biphasic model fits, the original criterion resulted in a median lifespan for short-lived infected cells of 3.3 days (SD = 7.2, n = 11), whereas the sustained criterion gave an estimate of 2.8 days (SD = 1.8, n = 6). The corresponding estimates for the lifespan of long-lived infected cells were 31.4 days (SD = 51.4, n = 11) and 28.1 days (SD = 16, n = 6). For the single phase model fits, the original and sustained criteria yielded median infected cell lifespans of 23.7 days (SD = 16.8, n = 32) and 26.3 days (SD = 20, n = 27), respectively. Therefore, athough the decay phases of seven individuals were noticeably slower using the sustained criterion (Figs. S7 and S8), using this more stringent definition of suppression did not substantially change our overall parameter estimates from either the single or biphasic model fits.

Using the original criterion we found an association between TTS and $\log_{10}$ baseline VL (correlation = 0.40, p = 0.01, n = 53) and a marginal association between TTS and baseline CD4 percentage (correlation = -0.36, p = 0.057). With the sustained criterion we only retained a marginal association with $\log_{10}$ baseline VL (correlation = 0.40, p = 0.053, n = 39). However the overall trends are similar between both criteria (Fig. S9).

Independent model fitting

We fit either the biphasic or single phase model to data from each infant using a maximum likelihood approach that assumes independent errors within the time series. If the independence assumption is violated, autocorrelation can arise amongst the model residuals and impact the associated standard errors. We used the `acf` function in R to test for autocorrelation in the model residuals for each of our fitted time series. We found no evidence for statistically significant autocorrelations in any of the infant data used in these analyses.

Nonlinear mixed effects approach

A nonlinear mixed effects (NLME) model was applied to all 53 infants who met our inclusion criteria. The biphasic equation (Eqn. 1) was first rescaled as follows:

$$\begin{aligned} V(t) &= A\exp(-\delta t) + B\exp(-\gamma t) \\ &= rV_0\exp^{-\delta t} + (1-r)V_0\exp^{-\gamma t}, \end{aligned} \tag{S6}$$

where $r = A/(A+B)$ and $V_0 = V(t=0) = A+B$. Equation S6 was then fit to the data using the `saemix` package in R [7], with fixed effects for r, V_0, γ, and δ and random effects for each infant. Log-normal distributions were assumed for V_0, δ, and γ, and a logit-normal distribution was assumed for the proportion r. All parameters were initially assumed to be independent; allowing δ and γ to be correlated (as found in the individual-based approach) did not substantially change our results. We used an exponential residual error model which assumes $V > 0$ and homoscedastic variance under log-transformation. The resulting model fits were in close agreement with the infant data (Fig. S10).

The estimated population parameters for the lifespans of short and long-lived infected cells, and the rescaled parameters r and V_0, were: 2.1 days (95% CI: 1.5–3.55 days), 34.2 days (29.5–40.8 days), 0.989 (0.983–0.996), and 48,700 copies ml^{-1}(16,300–81,100 copies ml^{-1}), respectively. In general, these overlapped the median estimates obtained from independently fitting the biphasic model to 11 infants (3.2 days, 31.4 days, 0.99, and 141,600 copies ml^{-1}, respectively). The distributions of the individual parameters were also similar to the original independent biphasic fits; for example, $r = A/(A+B)$ was highly skewed towards 0.99 (Fig. S11). Moreover, the maximum estimated short-lived infected cell lifespan was 13 days, and the minimum long-lived infected cell lifespan was 18.5 days. Thus our original cutoff value of 18 days (which we used to partition the independent short and long-lived estimates from the single phase model) also applies to the NLME parameter distributions.

Single phase lifespan partitioning

To partition the single phase lifespan estimates into those representing the short and long-lived infected cells, we defined a cutoff threshold of 18 days that was guided by the distribution of estimates from the biphasic model (see the main text and Fig. 3 for further details). To check the robustness of this approach, we investigated alternative partition criteria that classified single phase individuals based on when the majority of their measurements were observed. Specifically, we first calculated the timing of the phase transition for all biphasic individuals using Eqn. 2 (median = 22.0 days; IQR = 14.2–35.6). In general, measurements collected before this time represent the fast phase, and measurements after represent the slow phase. We then classified single phase trajectories as representing the fast phase if the majority (i.e. 50%) of their measurements were observed within 35.6 days (the upper interquartile of the biphasic fast phases).

This alternative method resulted in 12 trajectories being classified as fast phases and 20 as slow phases, corresponding to 12 short-lived and 20 long-lived lifespan estimates. Of these classifications, three short-lived estimates were classified as long-lived using the original method (SP23, SP25, SP32), and three long-lived estimates where originally classified as short-lived (SP3, SP12, SP28). Despite this small discrepancy, combining the alternative short and long-lived estimates with the corresponding biphasic partitions resulted in similar distributions to those obtained originally (alternative median short and long-lived lifespans = 7.1 days and 29.1 days, respectively, vs. original median short and long-lived lifespans = 7.1 days and 31.4 days, respectively).

Potential sampling bias of fast decay phases

In the main text we find that our estimates of the lifespan of short-lived infected cells are longer than reported in previous studies. There are a number of biological factors that could explain this result; however, an alternative explanation is that by only fitting the model to infants with sufficient data, our estimates are biased towards those with longer, and thus more well-documented, first decay phases.

To investigate this possibility further, we first note that shorter first phases are more likely to be unobserved if a faster first decay rate (δ) leads to an earlier phase switch, T_t. In other words, if an increase in δ leads to a decrease in T_t, i.e. $\frac{\partial}{\partial\delta}T_t < 0$. The timing of the phase switch is given by

$$T_t = \frac{\log(A\delta) - \log(B\gamma)}{\delta - \gamma}.$$

Setting $f(\delta) = \log(A\delta) - \log(B\gamma)$ and $g(\delta) = 1/(\delta - \gamma)$, the derivative of T_t with respect to δ is

$$\begin{aligned}
\frac{\partial}{\partial\delta}\Big(T_t\Big) &= f'g + g'f \\
&= \frac{1}{\delta}\frac{1}{(\delta-\gamma)} + \Big(-\frac{1}{(\delta-\gamma)^2}\Big)(\log(A\delta) - \log(B\gamma)) \\
&= \Big(\frac{1}{\delta-\gamma}\Big)\Big(\frac{1}{\delta} - \frac{\log(A\delta) - \log(B\gamma)}{(\delta-\gamma)}\Big) \\
&= \Big(\frac{1}{\delta-\gamma}\Big)\Big(\frac{\delta-\gamma}{\delta(\delta-\gamma)} - \frac{\delta(\log(A\delta) - \log(B\gamma))}{\delta(\delta-\gamma)}\Big) \\
&= \Big(\frac{1}{\delta(\delta-\gamma)^2}\Big)\Big(\delta - \gamma - \delta(\log(A\delta) - \log(B\gamma))\Big).
\end{aligned}$$

Since $\delta > 0$, the sign of $\frac{\partial}{\partial\delta}T_t$ is determined by $h(\delta, \gamma, A, B) = \delta - \gamma - \delta(\log(A\delta) - \log(B\gamma))$.

To determine the sign of $h(\delta, A, \gamma, B)$ around relevant parameter values, we first conducted a fine scale exploration by varying δ, γ, A and B between 90 – 110% of their median estimates from the biphasic model. We find that across all parameter values, $h(\delta, \gamma, A, B) < 0$ (Fig S12), and so $\frac{\partial}{\partial\delta}T_t < 0$. We then conducted a wider exploration of parameter space by varying δ, γ, A and B over the entire range of biologically plausible estimates from the biphasic model. Again we find that across all values, $h(\delta, \gamma, A, B) < 0$ (Fig S13), and so $\frac{\partial}{\partial\delta}T_t < 0$. Therefore, $\frac{\partial}{\partial\delta}T_t < 0$ across biologically relevant parameter values, and so our estimates of the lifespan of short-lived infected cells are likely biased towards those with longer, and thus more well-documented, first decay phases.

Supplementary figures and tables

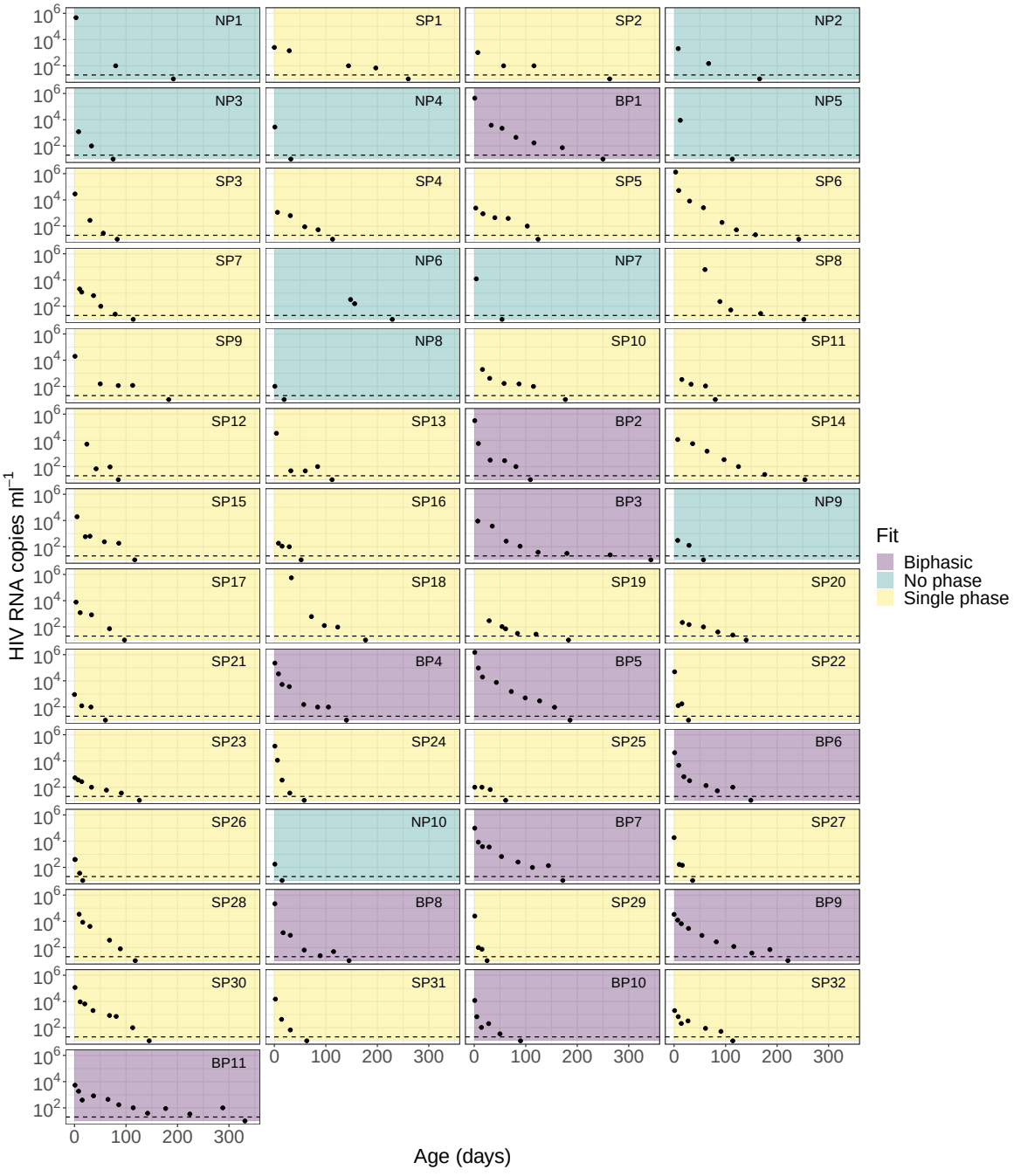

Figure S1: **53 infants that achieved suppression.** Each panel represents a different individual (IDs inset top right). Points represent the viral load data, and dashed horizontal lines indicate the detection threshold. Colors and IDs indicate whether the data were fit using the biphasic (BP) or single phase (SP) models, or whether neither model was fit and the infant was only included in non-parametric time to suppression calculations (NP). Data are shown until the first measurement below the detection threshold.

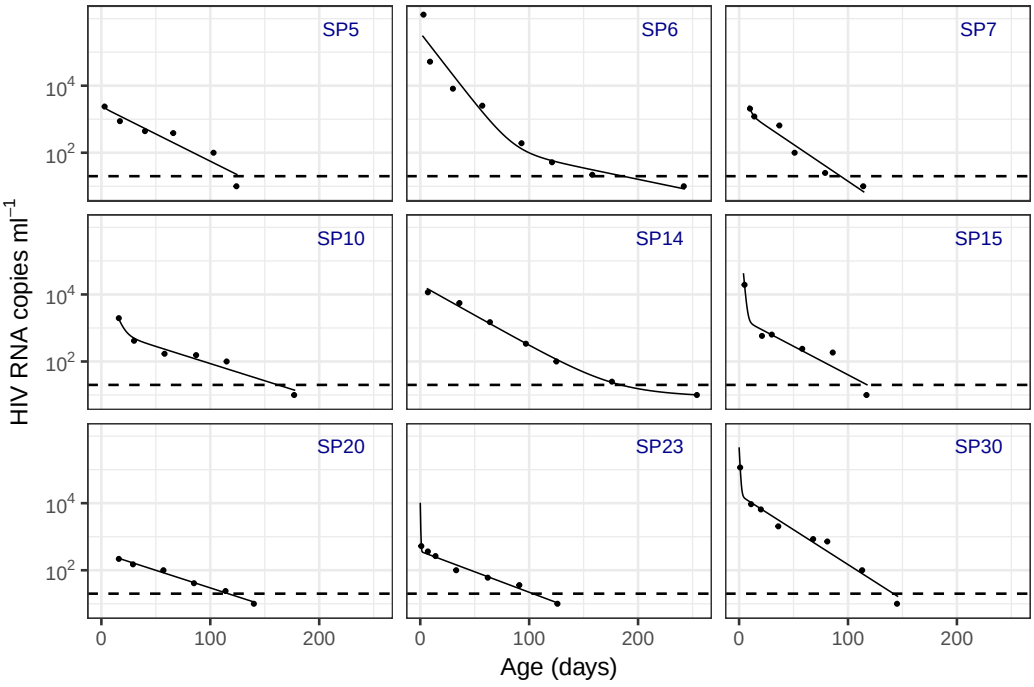

Figure S2: **Nine infants fit using the biphasic model with inadequate sampling.** Each panel represents a different infant (ID inset top right; 'SP' stands for single phase – the model ultimately used to fit these trajectories). Points represent the viral load data, solid lines are the biphasic model fit, and dashed horizontal lines indicate the detection threshold.

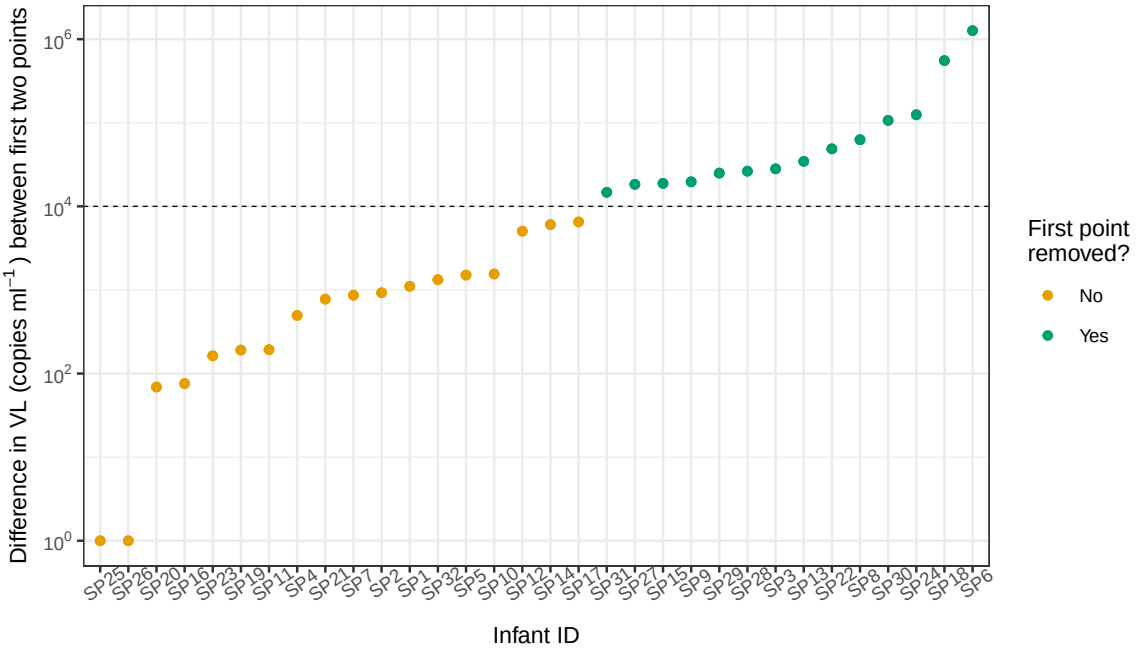

Figure S3: **Difference in viral load (VL) between first and second points.** The 32 single phase (SP) infants are represented by their corresponding ID; colors indicate whether the first data point was removed prior to model fitting. The 10^4 copies ml^{-1} removal threshold is depicted by the dashed line.

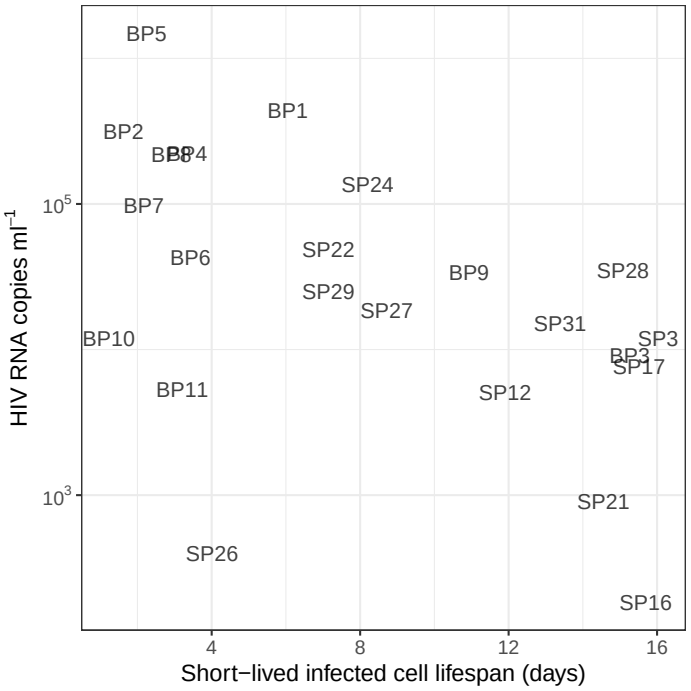

Figure S4: **Association between the lifespan of short-lived infected cells and baseline viral load.** The 11 short-lived lifespan estimates from the biphasic (BP) model were combined with 12 lifespan estimates from the single phase (SP) model that were below the cutoff threshold of 18 days. Individuals are represented by their respective IDs. Correlation = -0.56, $p = 0.03$.

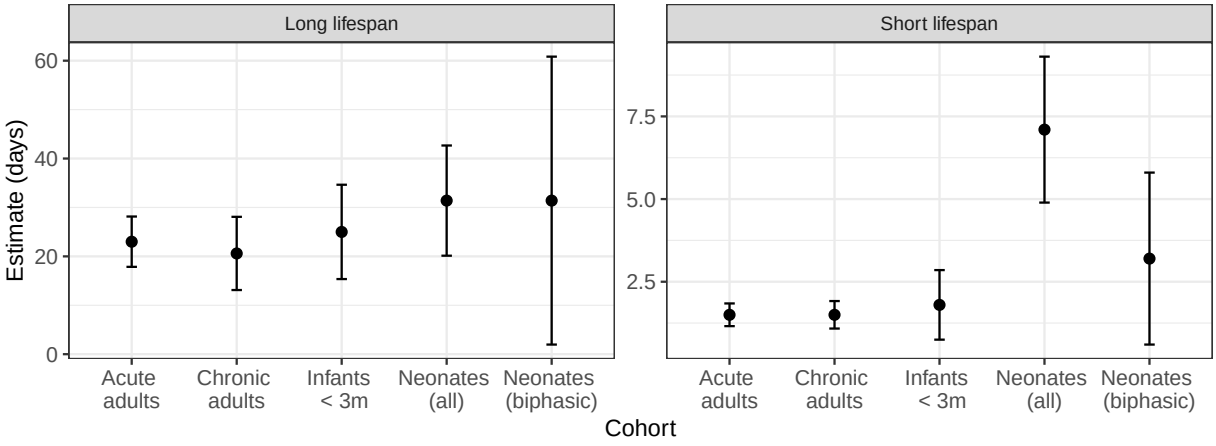

Figure S5: **Comparison of intra-study variation.** Points represent median estimates of the short (right) and long-lived (left) infected cell lifespans; errorbars represent approximate 95% confidence intervals (calculated as $\pm 1.96 \times \sigma / \sqrt{n}$, for standard deviation σ and sample size n). Representative estimates were collated from studies of acutely infected adults [8], chronically infected adults [9], and infants under three months of age [10]. These were compared to our combined estimates from the biphasic and single phase models ('Neonates (all)') and our estimates from just the biphasic model ('Neonates (biphasic)').

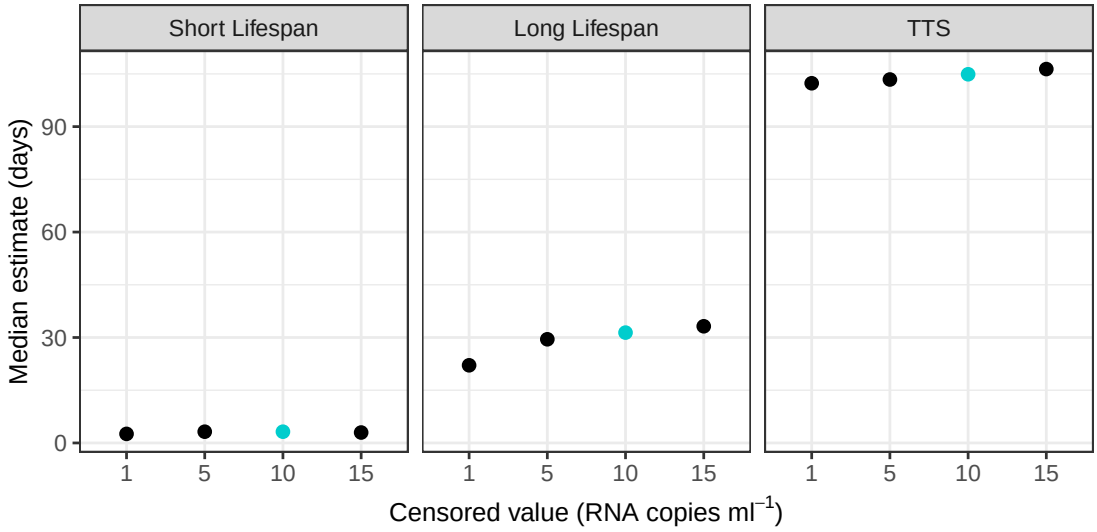

Figure S6: **Using alternative censoring values does not substantially change our results.** Points represent median estimates of the lifespan of short-lived infected cells (left panel), the lifespan of long-lived infected cells (middle panel), and the time to suppression (TTS, right panel) for different censoring values. The original value presented in the main text (10 copies ml^{-1}) is highlighted in blue.

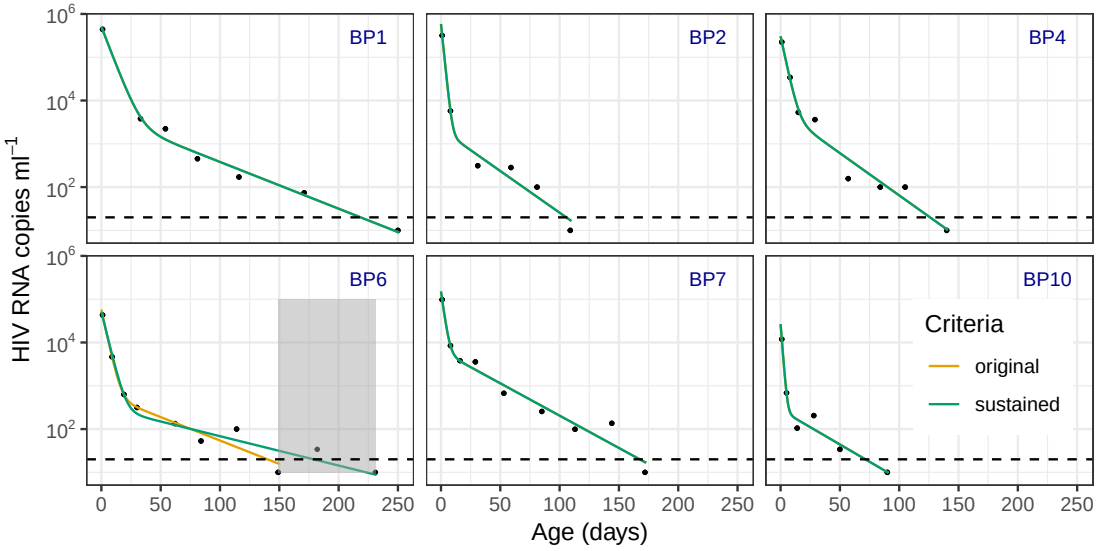

Figure S7: **Comparison of biphasic model fits for infants that fit both the original and sustained suppression criteria.** Each panel represents a different infant (ID inset top right; BP stands for 'biphasic'). Points represent the viral load data, solid lines are the model fits, and the dashed horizontal line indicates the detection threshold. Grey shaded regions show periods where additional data were included due to the more stringent sustained criteria. Infants for which there was no change in model fit have overlapping lines (and thus only one is visible).

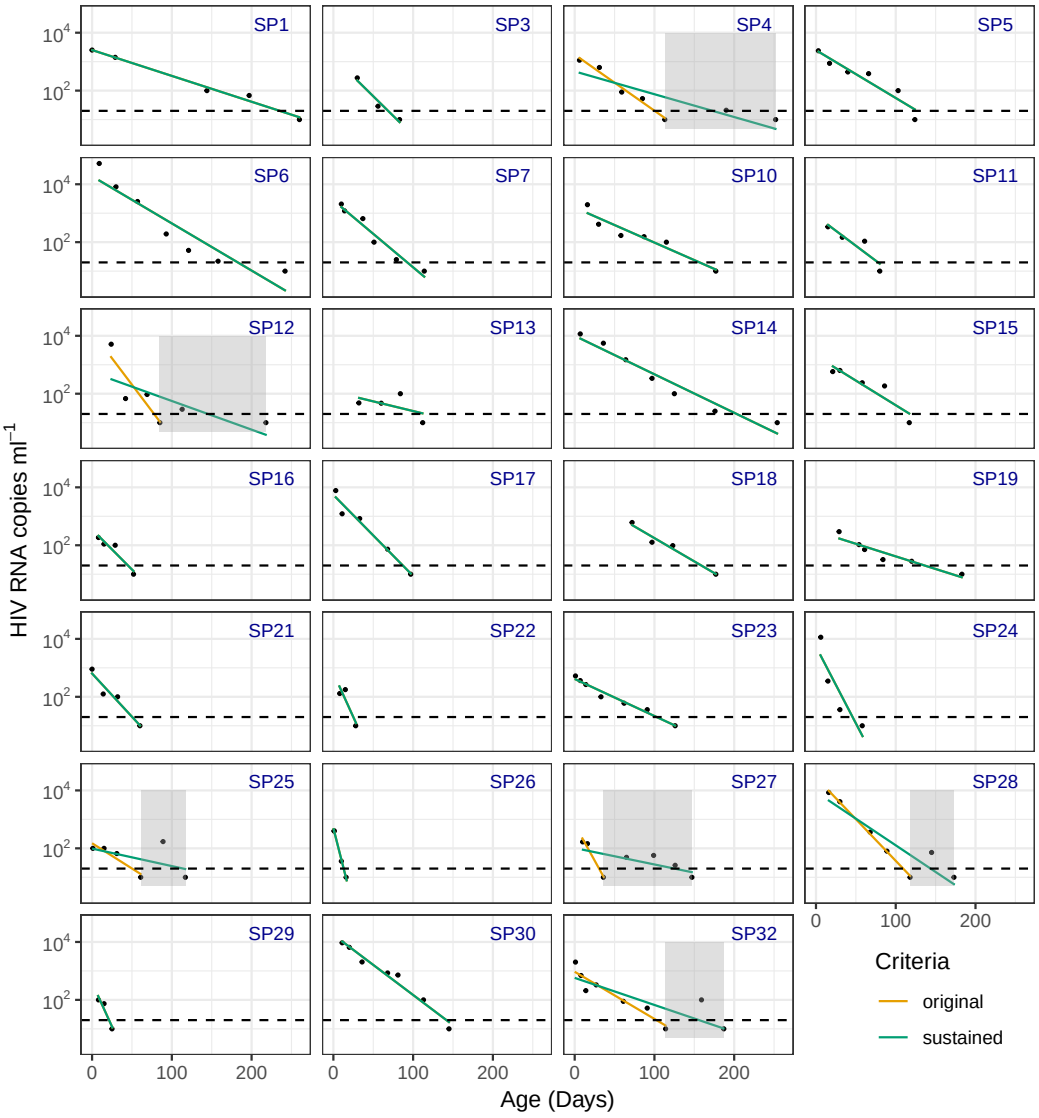

Figure S8: **Comparison of single phase model fits for infants that fit both the original and sustained suppression criteria.** Each panel represents a different infant (ID inset top right; SP stands for 'single phase'). Points represent the viral load data, solid lines are the model fits, and the dashed horizontal lines indicate the detection threshold. Grey shaded regions show periods where additional data were included due to the more stringent sustained criteria. Infants for which there was no change in model fit have overlapping lines (and thus only one is visible).

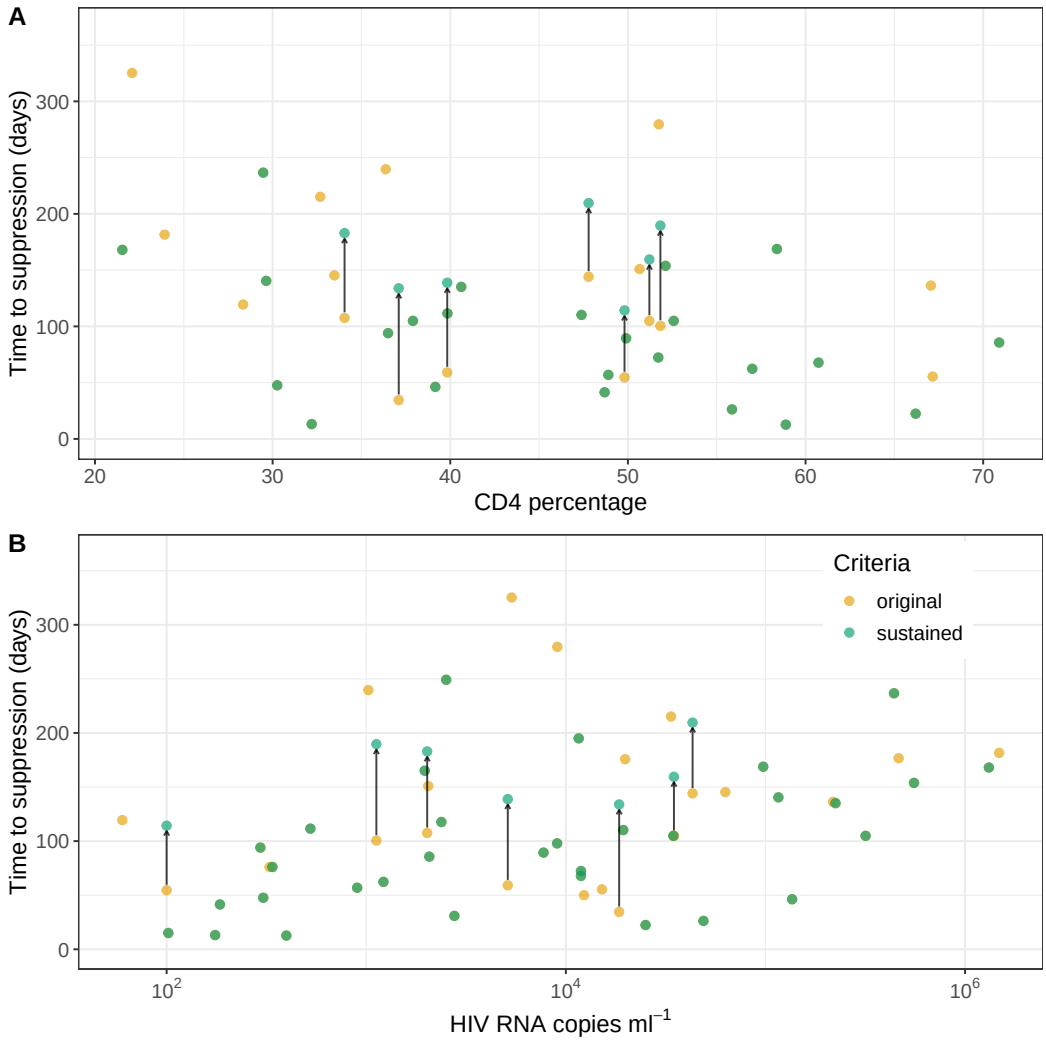

Figure S9: **Comparison of statistical associations for both the original and sustained suppression criteria.** Comparison of associations between time to suppression (TTS) and significant predictors in the original analysis, namely baseline CD4 percentage (A) and $\log_{10}$ viral load (B). Orange points show the original estimates and green points show the sustained estimates. Black arrows indicate the change in value from the original to the sustained criteria for the seven infants whose trajectories were altered. Orange points with no connecting arrow indicate infants that did not achieve sustained suppression and thus had no sustained estimate. Green points with no connecting arrow overlap their corresponding orange points, indicating no change in estimate.

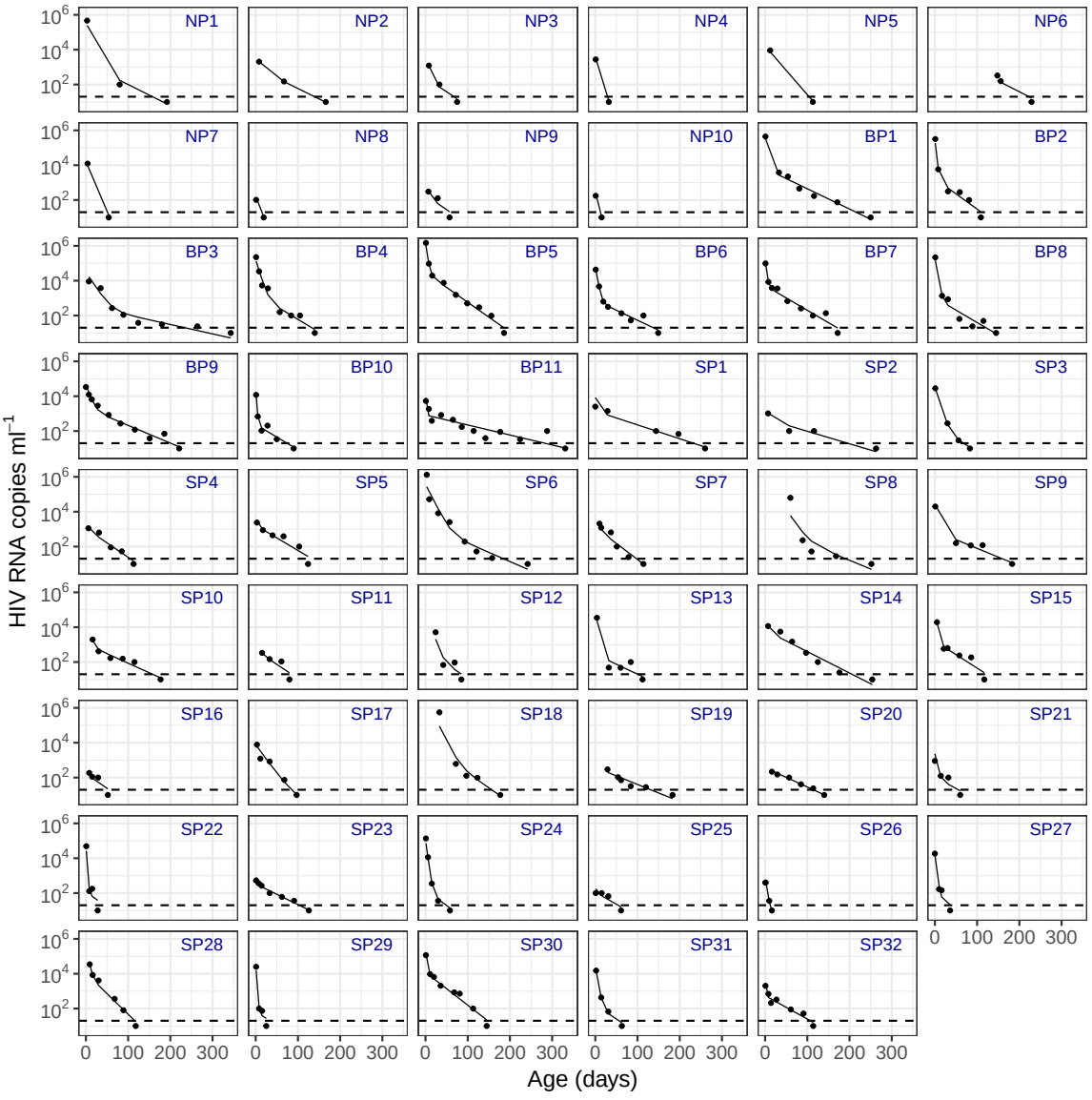

Figure S10: **53 infants fit using a nonlinear mixed effects (NLME) approach.** Each panel represents a different infant (ID inset top right). Infant IDs are as in the main text and correspond to the individual-based fitting results: BP for 'biphasic', 'SP' for single phase, and 'NP' for no phase (i.e. neither model was fit). Points represent the viral load data, solid lines are the NLME biphasic model fits, and dashed horizontal lines indicate the detection threshold.

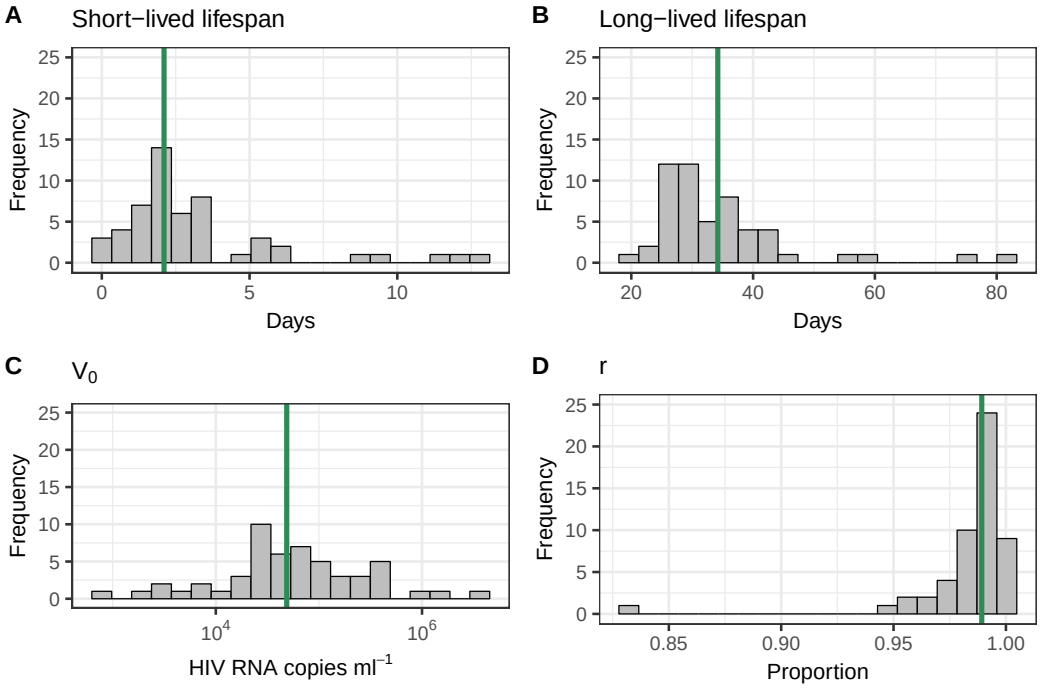

Figure S11: **Individual parameter distributions from the nonlinear mixed effects model.** Distributions for the short-lived infected cell lifespan (A), the long-lived infected cell lifespan (B), $V_0 = A + B$ (C), and $r = A/(A + B)$ (D). The green vertical lines represent the corresponding population parameter estimates.

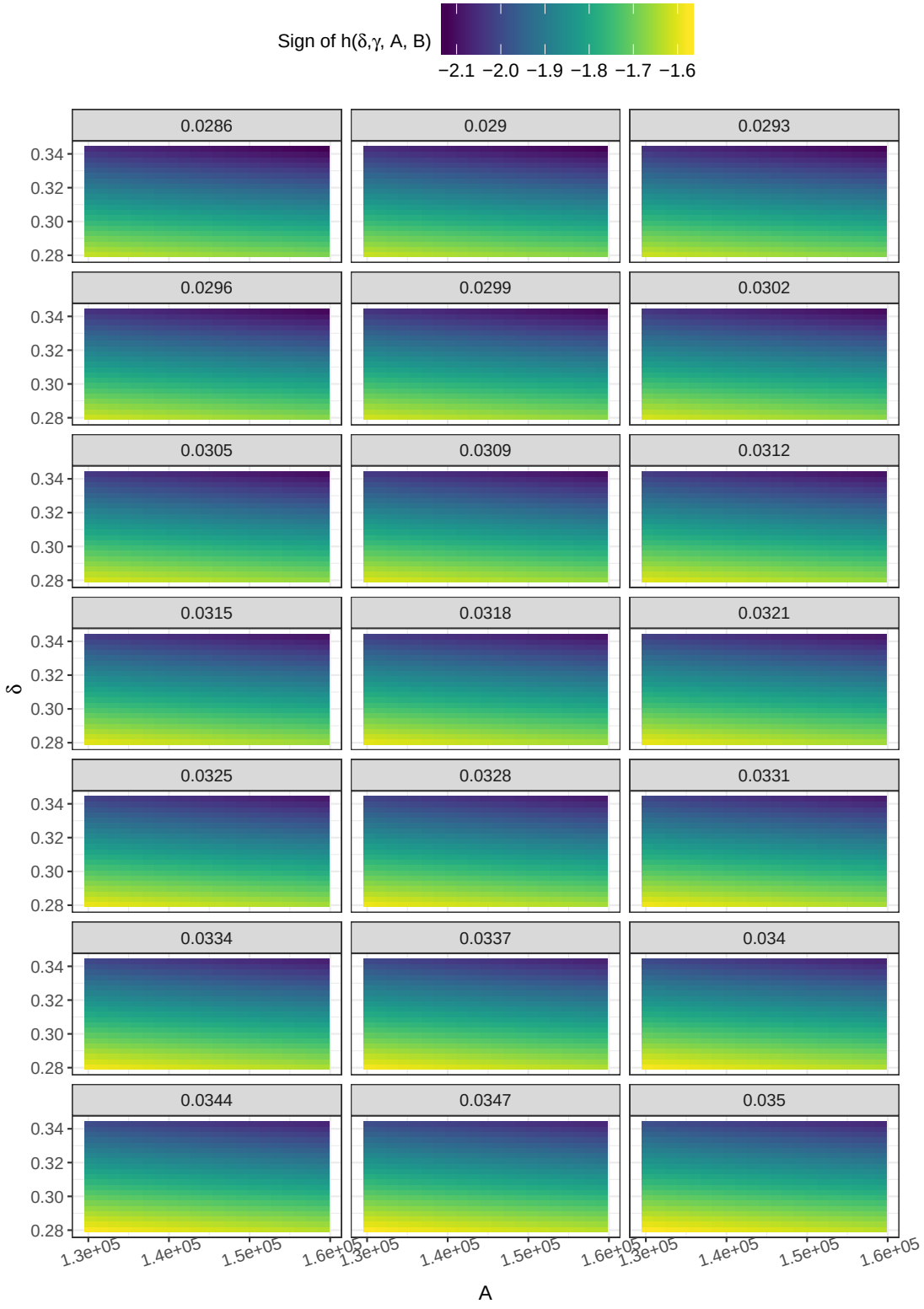

Figure S12: **Sampling bias potential over a narrow parameter range.** The parameters δ, γ, A and B were varied between 90 - 110% of their median estimates from the biphasic model. For clarity, the plot shows representative results for a fixed value of B = 1567 (its median estimate from the biphasic model). Each panel represents a different value of γ, and colors represent the sign of $h(\delta, \gamma, A, B) = \delta - \gamma - \delta(\log(A\delta) - \log(B\gamma))$.

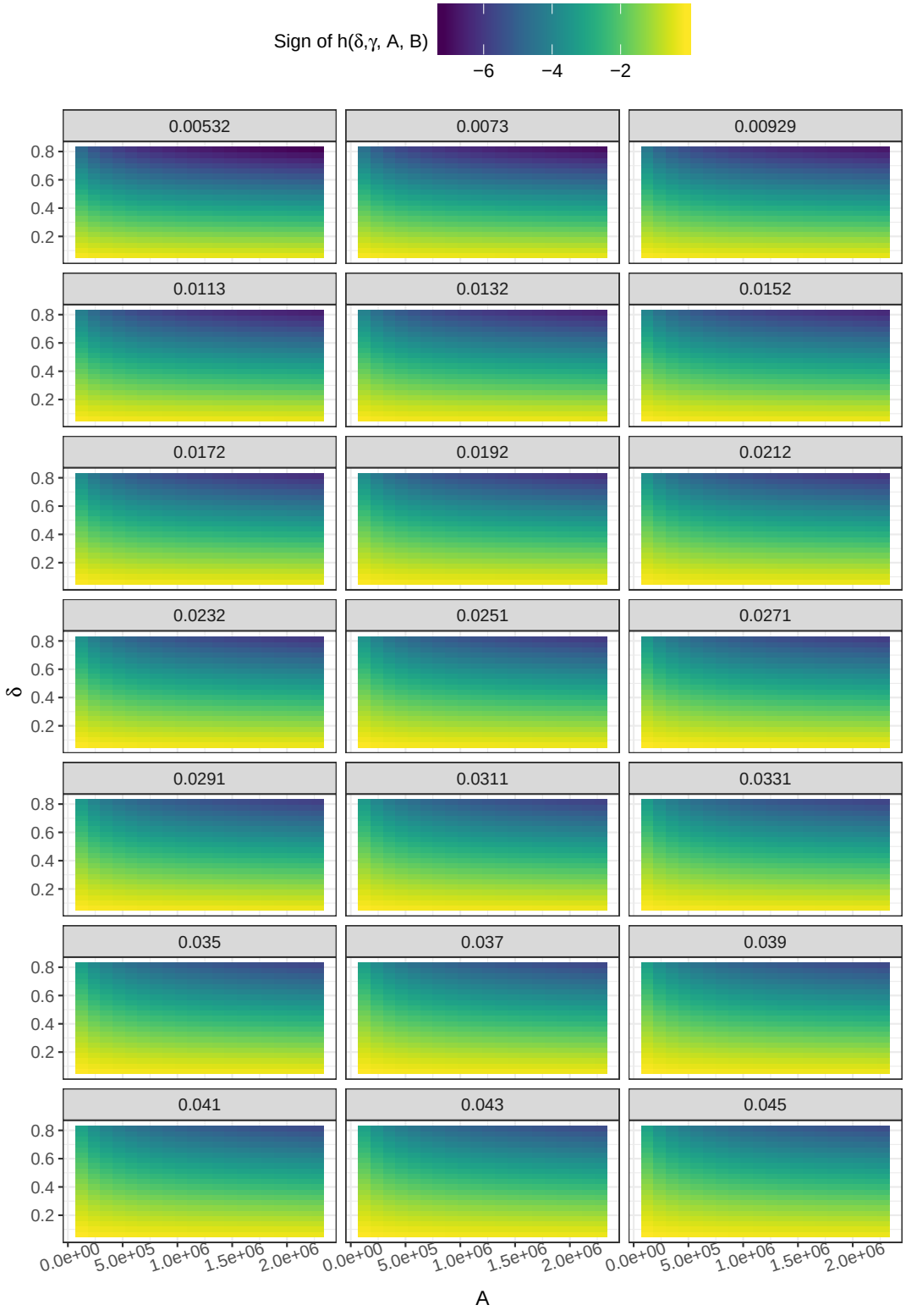

Figure S13: **Sampling bias potential over a wide parameter range.** The parameters δ, γ, A and B were varied between their minimum and maximum estimates from the biphasic model. For clarity, the plot shows representative results for a fixed value of B = 19407 (the midpoint between its minimum and maximum biphasic estimates). Each panel represents a different value of γ, and colors represent the sign of $h(\delta, \gamma, A, B) = \delta - \gamma - \delta(\log(A\delta) - \log(B\gamma))$.

Table S1: Parameter estimates (and 95% confidence intervals) for 11 infants fit using the biphasic (BP) model.

Infant ID	A (copies ml^{-1})	B (copies ml^{-1})	$1/\delta$ (days)	$1/\gamma$ (days)
BP1	5.0×10^5 (2.7×10^5 - 9.3×10^5)	4.6×10^3 (2.4×10^3 - 8.6×10^3)	6.1 (4.5 - 8.2)	40.2 (34.2 - 47.3)
BP2	5.8×10^5 (2.1×10^5 - 1.6×10^6)	2.2×10^3 (6.7×10^2 - 6.9×10^3)	1.6 (1.1 - 2.3)	22.6 (15.9 - 31.9)
BP3	1.9×10^4 (1.1×10^4 - 3.5×10^4)	7.5×10^1 (2.9×10^1 - 1.9×10^2)	15.3 (12.4 - 18.8)	187.9 (91.7 - 385)
BP4	3.0×10^5 (9.0×10^4 - 1.0×10^6)	5.8×10^3 (1.8×10^3 - 1.9×10^4)	3.3 (1.8 - 6.2)	22.2 (16.7 - 29.6)
BP5	2.3×10^6 (1.1×10^6 - 4.6×10^6)	3.9×10^4 (2.4×10^4 - 6.4×10^4)	2.2 (1.6 - 3.1)	24 (21.7 - 26.6)
BP6	5.7×10^4 (2.4×10^4 - 1.3×10^5)	6.6×10^2 (2.9×10^2 - 1.5×10^3)	3.4 (2.3 - 5.2)	40.1 (28.4 - 56.7)
BP7	1.4×10^5 (4.4×10^4 - 4.7×10^5)	6.4×10^3 (3.2×10^3 - 1.3×10^4)	2.2 (1 - 4.8)	29.1 (24 - 35.3)
BP8	3.0×10^5 (8.0×10^4 - 1.1×10^6)	9.3×10^2 (2.4×10^2 - 3.6×10^3)	2.9 (1.8 - 4.8)	31.4 (20.3 - 48.8)
BP9	2.5×10^4 (1.3×10^4 - 4.5×10^4)	1.6×10^3 (4.4×10^2 - 5.6×10^3)	10.9 (5.8 - 20.4)	46.9 (32.7 - 67.2)
BP10	2.6×10^4 (1.0×10^4 - 6.8×10^4)	2.8×10^2 (1.4×10^2 - 5.5×10^2)	1.2 (0.8 - 1.9)	27.2 (19.3 - 38.2)
BP11	1.1×10^4 (2.5×10^3 - 5.1×10^4)	5.2×10^2 (2.4×10^2 - 1.1×10^3)	3.2 (1.3 - 7.7)	95.4 (63.6 - 143)
Median (SD)	1.4×10^5 (6.6×10^5)	1.6×10^3 (1.1×10^4)	3.2 (4.4)	31.4 (49.8)

Table S2: Parameter estimates (and 95% confidence intervals) for 32 infants fit using the single phase (SP) model.

Infant ID	$\hat{B}$ (copies ml^{-1})	$1/\hat{\gamma}$ (days)
SP1	2.5×10^3 (1.8×10^3 - 3.6×10^3)	48.7 (43.8 - 54.1)
SP2	6.0×10^2 (2.6×10^2 - 1.4×10^3)	62.3 (43.9 - 88.3)
SP3	1.4×10^3 (5.7×10^2 - 3.7×10^3)	16 (12.5 - 20.5)
SP4	1.8×10^3 (1.1×10^3 - 2.7×10^3)	22.4 (19.4 - 25.9)
SP5	2.5×10^3 (1.2×10^3 - 5.2×10^3)	26.3 (20.3 - 34.1)
SP6	1.9×10^4 (5.0×10^3 - 7.2×10^4)	26.7 (20.1 - 35.4)
SP7	2.8×10^3 (1.5×10^3 - 5.1×10^3)	18.8 (15.7 - 22.5)
SP8	5.7×10^2 (1.9×10^2 - 1.7×10^3)	59.9 (40.4 - 88.8)
SP9	6.7×10^2 (2.4×10^2 - 1.8×10^3)	47.3 (31.6 - 70.7)
SP10	1.6×10^3 (8.1×10^2 - 3.1×10^3)	35.9 (28.1 - 45.8)
SP11	8.1×10^2 (2.6×10^2 - 2.5×10^3)	21 (13.4 - 32.8)
SP12	1.4×10^4 (8.7×10^2 - 2.1×10^5)	11.9 (6.9 - 20.6)
SP13	1.2×10^2 (1.9×10^1 - 7.3×10^2)	65 (14.2 - 297.3)
SP14	1.0×10^4 (4.9×10^3 - 2.1×10^4)	32.7 (27.4 - 39)
SP15	2.0×10^3 (7.2×10^2 - 5.6×10^3)	25.5 (17.7 - 36.8)
SP16	3.5×10^2 (1.9×10^2 - 6.5×10^2)	15.7 (11.5 - 21.5)
SP17	5.5×10^3 (3.0×10^3 - 1.0×10^4)	15.5 (13.1 - 18.4)
SP18	7.2×10^3 (3.1×10^3 - 1.7×10^4)	27 (22.4 - 32.5)
SP19	3.1×10^2 (1.7×10^2 - 5.4×10^2)	49.9 (37.8 - 65.9)
SP20	3.3×10^2 (2.8×10^2 - 4.0×10^2)	41.4 (38.1 - 45)
SP21	6.4×10^2 (3.4×10^2 - 1.2×10^3)	14.6 (11.2 - 18.9)
SP22	6.6×10^2 (1.6×10^2 - 2.8×10^3)	7.1 (4.1 - 12.3)
SP23	4.1×10^2 (3.2×10^2 - 5.3×10^2)	34 (29.9 - 38.6)
SP24	5.4×10^3 (7.7×10^2 - 3.8×10^4)	8.2 (5.1 - 13.2)
SP25	1.5×10^2 (9.1×10^1 - 2.5×10^2)	24.9 (17.5 - 35.5)
SP26	5.0×10^2 (4.4×10^2 - 5.6×10^2)	4 (3.8 - 4.2)
SP27	6.7×10^2 (3.9×10^2 - 1.2×10^3)	8.7 (7.1 - 10.7)
SP28	2.8×10^4 (2.3×10^4 - 3.4×10^4)	15.1 (14.5 - 15.7)
SP29	3.9×10^2 (1.7×10^2 - 9.3×10^2)	7.1 (5 - 10.2)
SP30	1.8×10^4 (1.1×10^4 - 3.0×10^4)	20.9 (18.3 - 23.8)
SP31	9.7×10^2 (5.4×10^2 - 1.8×10^3)	13.4 (11 - 16.3)
SP32	9.3×10^2 (5.2×10^2 - 1.7×10^3)	26.7 (20.7 - 34.4)
Median (SD)	9.5×10^2 (6.6×10^3)	23.7 (16.8)

Table S3: Non-parametric time to suppression (TTS) summary statistics with respect to baseline covariates, for all 53 infants included in the analysis.

Covariate	Group	Median	Mean	SD	N
Age at ART initiation (days)	<2d	107.5	114.8	83.5	25
	From 2-14d	104.9	116.2	66.7	22
	Over 14d	95.9	104.4	37.7	6
Birthweight (g)	<2500	104	116.7	55.2	14
	2500+	104.9	113.3	77.6	39
Delivery mode	Emergency CS	117.7	122.1	64.4	17
	NVD	95.9	110.5	75.7	36
Baseline CD4 count (cells mm^{-3})	<1500	110.2	143.8	88.1	9
	1500+	104.9	104.2	66.3	32
	No measurement*	107.8	118.8	73.1	12
Baseline CD4 percentage	<35	145.3	154.6	87	11
	35+	91.7	97.6	60.9	30
	No measurement*	107.8	118.8	73.1	12
Baseline viral load (copies ml^{-1})	<2,000	69.2	80.4	59.5	16
	2,000-10,000	107.5	144.8	96.4	11
	10,000-100,000	104.9	105.8	62.4	16
	100,000+	147.1	148	50.4	10
Preterm status	No	104.9	115.2	77.6	43
	Yes	102.7	109.8	41.1	10
Sex	Female	85.7	109.1	81.6	27
	Male	106.2	119.5	61.3	26
Mother's age (years)	<30	110.2	120.7	76	33
	30+	101.4	103.5	64.8	20
Mother's CD4 count (cells mm^{-3})	<350	97.9	100.4	66.1	21
	350+	114.6	123.3	75	32
Mother's PMTCT status	No	111.3	107.5	62.3	16
	Yes	100.5	117.1	76.2	37
Mother's viral load (copies ml^{-1})	<1000	99.2	104.7	65.8	18
	1000+	110.2	119	75.2	35
Mother's PMTCT status & viral load (copies ml^{-1})	No	111.3	107.5	62.3	16
	Yes, <1000	94	99.1	69.7	15
	Yes, 1000+	110.9	129.3	79.6	22

*The 12 infants without CD4 count measurements are the same 12 infants without CD4 percentage measurements.

CS = cesarean section; NVD = normal vaginal delivery; PMTCT = prevention of mother-to-child transmission.

References

1. Wu H, Ding AA. Population HIV-1 dynamics in vivo: applicable models and inferential tools for virological data from AIDS clinical trials. *Biometrics*. 1999;55(2):410–418. doi:10.1111/j.0006-341x.1999.00410.x.

2. Perelson AS, Neumann AU, Markowitz M, et al. HIV-1 dynamics in vivo: virion clearance rate, infected cell life-span, and viral generation time. *Science*. 1996;271(5255):1582–1586. doi:10.1126/science.271.5255.1582.

3. Nowak MA, May RM. *Virus Dynamics: Mathematical Principles of Immunology and Virology*. New York,USA: Oxford University Press; 2000.

4. Shet A, Nagaraja P, Dixit NM. Viral decay dynamics and mathematical modeling of treatment response: evidence of lower in vivo fitness of HIV-1 subtype C. *J Acquir Immune Defic Syndr*. 2016;73(3):245–251. doi:10.1097/QAI.0000000000001101.

5. Wu H, Connick E, Kuritzkes DR, et al. Multiple CD4+ cell kinetic patterns and their relationships with baseline factors and virological responses in HIV type 1 patients receiving highly active antiretroviral therapy. *AIDS Res Hum Retroviruses*. 2001;17(13):1231–1240. doi:10.1089/088922201750461285.

6. Wu H, Kuritzkes DR, McClernon DR, et al. Characterization of viral dynamics in human immunodeficiency virus type 1-infected patients treated with combination antiretroviral therapy: relationships to host factors, cellular restoration, and virologic end points. *J Infect Dis*. 1999;179(4):799–807. doi:10.1086/314670.

7. Comets E, Lavenu A, Lavielle M. Parameter estimation in nonlinear mixed effect models using saemix, an R implementation of the SAEM algorithm. *J Stat Softw*. 2017;80(3):1–41. doi:10.18637/jss.v080.i03.

8. Kilby JM, Lee HY, Hazelwood JD, et al. Treatment response in acute/early infection versus advanced AIDS: equivalent first and second phases of HIV RNA decline. *AIDS*. 2008;22(8):957–962. doi:10.1038/jid.2014.371.

9. Perelson AS, Essunger P, Cao Y, et al. Decay characteristics of HIV-1-infected compartments during combination therapy. *Nature*. 1997;387(6629):188–191. doi:10.1038/387188a0.

10. Luzuriaga K, Wu H, McManus M, et al. Dynamics of human immunodeficiency virus type 1 replication in vertically infected infants. *J Virol*. 1999;73(1):362–367. doi:10.1128/JVI.73.1.362-367.1999.